# 3D Brain Surface Matching Based on Geodesics and Local Geometry

**Yongmei Wang***

Department of Information Engineering

The Chinese University of Hong Kong

Shatin, N.T., Hong Kong

E-mail: ymwang@ie.cuhk.edu.hk

Tel: (+852) 2609 8483 ; Fax: (+852) 2603-5032

**Bradley S. Peterson**

Child Study Center

Yale University, New Haven, CT 06520

**Lawrence H. Staib**

Departments of Electrical Engineering and Diagnostic Radiology

Yale University

P.O. Box 208042, New Haven, CT 06520-8042

E-mail: lawrence.staib@yale.edu

*Corresponding Author.

# Abstract

This paper presents a new approach for 3D brain surface matching based on shape using a combination of geodesic distance and surface curvature. An initial sparse set of corresponding points are first generated by matching local geometrical features. Geodesic interpolation is then employed in order to capture the complex surface. In addition, surface correspondence and triangulation are computed simultaneously through a hierarchical scheme. Experiments applied to human cerebral cortical surfaces are shown to evaluate the approach. It is shown that the proposed method performs well for both surface matching and surface shape recovery.



**Keywords:** surface matching, correspondence, corresponding points, geodesics, geometrical features, shortest paths, shape, triangulation.

# 1 Introduction

The shape analysis of the human cerebral cortex is of tremendous interest to neuroscientists trying to understand the relationship between morphologic differences and behavioral and psychological factors in normal individuals and in those with disorders. For example, cortical differences associated with sex [25], age [14] and cognitive abilities [15] have been found and are studied in order to understand normal development. Differences have also been associated with many neurologic and psychiatric disorders and are key to understanding abnormalities in regions or systems associated with these disorders. The measurement of brain structure has revealed cortical abnormalities associated with conditions such as Alzheimer's disease [28], schizophrenia [37], dyslexia [31], panic disorder [24] and in preterm infants [26].

The detailed comparison of different human brains requires nonrigid registration of surfaces, or surface matching. This can be achieved by determining the correspondence of 3D point sets between pairs of surfaces. While shape provides the basis for such a correspondence, this problem remains a difficult one due to ambiguity when the surfaces are complex and variable. In addition, the lack of ground truth for matching / correspondence remains a problem for evaluating such methods.

A number of methods have been developed to match surfaces and to determine surface correspondence. The classic approach is the iterative closest point method (ICP) [1]. This method (and related ones [9]) minimize the distance from points in one surface to the closest point in another surface. The robust point matching approach of Rangarajan *et al.* [27] also uses distance and has the advantage of establishing the correspondence between two sets of points in a robust way, discarding outlier points. Neither approach, however, explicitly uses shape to determine this match. ICP has been improved with shape information for sulcal model building [5].

Others determine surface correspondence by finding a continuous mapping for the purposes

of determining a full 3D volumetric deformation. Davatzikos *et al.* [7] determine a map from one surface to another by elastically reparametrizing one of the surfaces so that geometric features align. This work has been extended by explicitly constraining sulcal and gyral curve matches [40]. Thompson and Toga [39] formulate warping using Chen surfaces (hybrid superquadrics and spherical harmonics) to extract surface models of structure, including sulci. Other related work in nonrigid volumetric transformation include [6, 35, 11].

A surface correspondence algorithm is also developed in [10] to build a statistical shape model. In this method, random point sets on the surface are identified first, and then these clouds of points are registered and matched to establish correspondence using a multi-resolution octree spline approach. The accuracy of the correspondence is dependent on the registration process, which is very computationally expensive and may not be sufficiently flexible for complex deformations. In addition, a further surface triangulation method is needed to form a surface from the unorganized points.

In our approach, we use curvature as part of the matching criterion. Matching of shape based on curvature has also been used for non-rigid motion tracking [8]. Shi *et al.* [36] use shape-based correspondence for analyzing left-ventricular motion. Note that for motion, the problem of correspondence is much more constrained due to the incremental change in shape between time frames. Other methods are designed particularly for matching curves in 2D [38, 23] and may not extend easily to 3D.

Geodesic distance is an important geometric measure for understanding complex shape and is a key component of our approach. One of the first uses in brain analysis was by Griffin [13] who used mean geodesic distance to characterize cortical shape. Geodesic distance and curvature have also been used to follow sulci [44, 17, 29]. The cortical surface is composed of folds (gyri) separated by sulci. The geodesic path connecting points in a sulcus will tend to follow the sulcus. Recently, minimal paths constructed across the surface have also been used

for surface patch parameterization [3].

# 2 Algorithm Overview

We propose a new automatic method using shape-based matching and geodesic interpolation to directly identify corresponding points on pairs of brain surfaces [42]. An individual (or study) surface is matched to a reference (or atlas) surface. This method simultaneously triangulates the study surface based on the generated points. An initial sparse set of points on the study surface are determined based on proximity and shape. The interpolated points in 3D are then generated by finding the shortest surface paths between the initial points and then labeling the interpolated points equally spaced along these paths. Given corresponding surface points, it is necessary to triangulate these 3D points to visualize and validate the surface. Our surface mapping algorithm also triangulates the brain surface during the identification of corresponding surface points by using a hierarchical scheme (Figure 1). The detailed steps of our approach are described in the next Section.

# 3 Our Approach

## 3.1 Initial Points Matching and Triangulation

This algorithm starts with segmented brain images, which can be determined either manually or automatically. Triangulated surfaces (at the level of voxel size) can be extracted from the segmented images using the Marching Cube algorithm [22].

### 3.1.1 Initial Points Labeling on the Atlas

First, a small set of points on an atlas brain surface is labeled manually. These points are normally sulcal, gyral or other feature points, which would be visually identifiable from a 3D

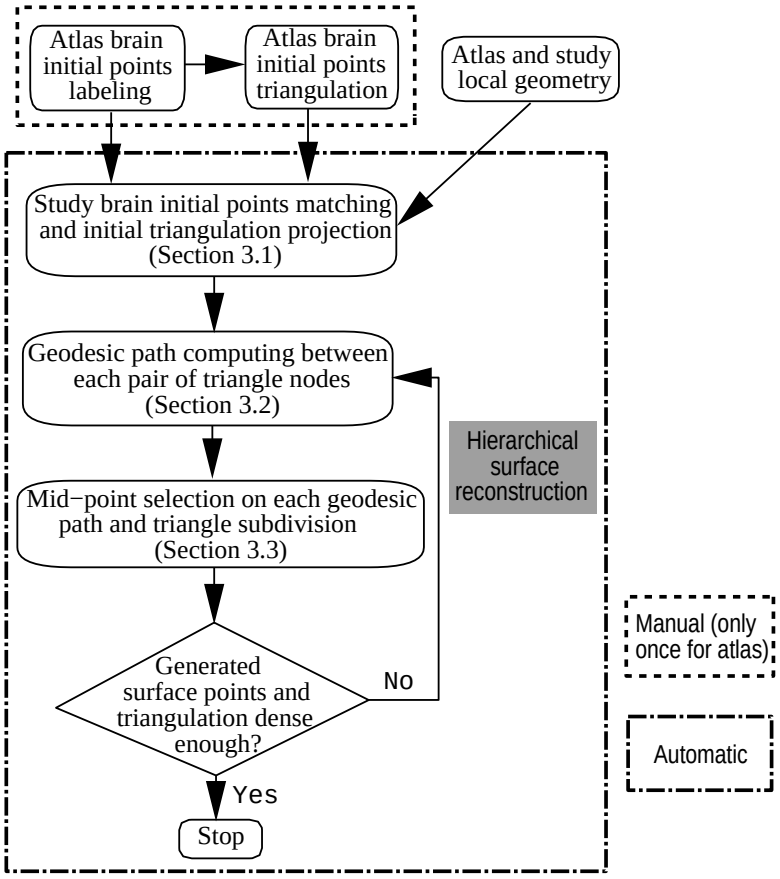


Figure 1: System framework of our hierarchical algorithm.

rendering. In order to match these points more accurately in the study brain, we divide the atlas initial points into four varieties according to their positions in the brain: $l = 1$ for inter-hemispheric fissure sulcal points; $l = 2$ for creases at the brain stem and cerebellum; $l = 3$ for the remaining sulcal points; $l = 4$ for gyral points. An initial triangulation of these points is constructed manually. This manual step only needs to be done once for the atlas image.

### 3.1.2 Corresponding Initial Points on the Study

For each individual study brain, we use the following automatic method to determine the corresponding points of the atlas. The initial triangle connections are inherited from the atlas.

First, we align the study to the atlas by scaling, translation and rotation. The Procrustes

shape distance method [2] is adopted here to calculate the scaling parameter using several thousand points evenly sampled on the two surfaces. Rigid registration is then performed using distance transform methods [16].

The procedure for determining the initial corresponding points of the atlas is based on an objective function matching local geometry (Eq.(1)). For each initial point $i$ on the atlas surface, the objective function to be minimized within a region for point $j$ on the study surface is:

$$O_{ij} = d_{ij} \cdot n_{ij} \cdot f_{ij} \tag{1}$$

where $d_{ij}$, $n_{ij}$ and $f_{ij}$ are respectively, a Euclidean distance measure, a surface normal match measure and a 21 feature (curvedness) match measure, formulated as follows.

The **Euclidean distance measure** is defined as:

$$d_{ij} = 1 + \sqrt{[x_i - x_j]^2 + [y_i - y_j]^2 + [z_i - z_j]^2} \tag{2}$$

where $(x, y, z)$ is the 3D co-ordinates for each surface point. Note that $1 \leq d_{ij} \leq R_w$, where $R_w$ is the radius of the search window with center point $i$. While a fixed radius is used here, a coarse to fine search strategy can be achieved by using gradually decreased window size.

The **surface normal match measure** is defined as:

$$n_{ij} = 2 - \vec{n}_i \cdot \vec{n}_j \tag{3}$$

where $\vec{n}$ is the unit normal vector for each surface point. Note that $1 \leq n_{ij} \leq 3$.

The **feature match measure** is defined in terms of curvedness.

Given the segmented brain image $L$, the Gaussian curvature, $K$, and the mean surface curvature, $H$, can be calculated from the partial derivatives of the image as [30, 34, 43]:

$$\begin{aligned} K &= \frac{\sum_{(i,j,k)\in\Omega} \left[L_i^2(L_{jj}L_{kk} - L_{jk}^2) + 2L_iL_j(L_{ik}L_{jk} - L_{ij}L_{kk})\right]}{(L_i^2 + L_j^2 + L_k^2)^2}; \\ H &= \frac{\sum_{(i,j,k)\in\Omega} \left[(L_{ii} + L_{jj})L_k^2 - 2L_iL_jL_{ij}\right]}{2(L_i^2 + L_j^2 + L_k^2)^{3/2}} \end{aligned} \tag{4}$$

where $\Omega = \{(x, y, z), (y, z, x), (z, x, y)\}$ is the set of circular shifts of $(x, y, z)$.

The two principal curvatures $k_1$ and $k_2$ are related to the Gaussian and mean curvatures as [4]: $k_1 = H + \sqrt{H^2 - K}$, and $k_2 = H - \sqrt{H^2 - K}$. Shape can be characterized by two values: one describing the type of curvature and one describing the degree [21]. A shape index function, defined as $S = \frac{2}{\pi} \arctan[(k_2 + k_1)/(k_2 - k_1)]$, can be used to classify surfaces into nine types [21]. Shape index distinguishes between sulci and gyri [43]. Curvedness measures the degree of curvature [21]: $C = \sqrt{(k_1^2 + k_2^2)/2}$.

In our matching procedure, we would like to locate sulcal and gyral points, $t$, by thresholding a signed curvedness, $C_s$, defined as:

$$C_s = \begin{cases} \sqrt{\frac{k_1^2+k_2^2}{2}}, & \text{if } S \geq 0 \\ -\sqrt{\frac{k_1^2+k_2^2}{2}}, & \text{if } S < 0 \end{cases} \tag{5}$$

Then,

$$t = \begin{cases} \text{gyrus}, & \text{if } C_s > K_g \\ \text{sulcus}, & \text{if } C_s < -K_s \\ \text{no feature}, & \text{otherwise} \end{cases} \tag{6}$$

The threshold values $K_g$ and $K_s$ are chosen dynamically so that the selected sulcal or gyral points are approximately a specified percentage of the total surface points (see Figure 2 for detailed percentages, fixed for each scale). Also, in order to locate these points more accurately, we empirically identify them at three scales according to their labeling $l$ in the atlas specified above:

$$scale = \begin{cases} 1, & \text{if } l = 3 \text{ or } 4 \\ 2, & \text{if } l = 1 \\ 3, & \text{if } l = 2 \end{cases} \tag{7}$$

Due to variations in shape, points with different labels, $l$, are more consistent when measured at their respective scales, which can be seen in Figure 2.

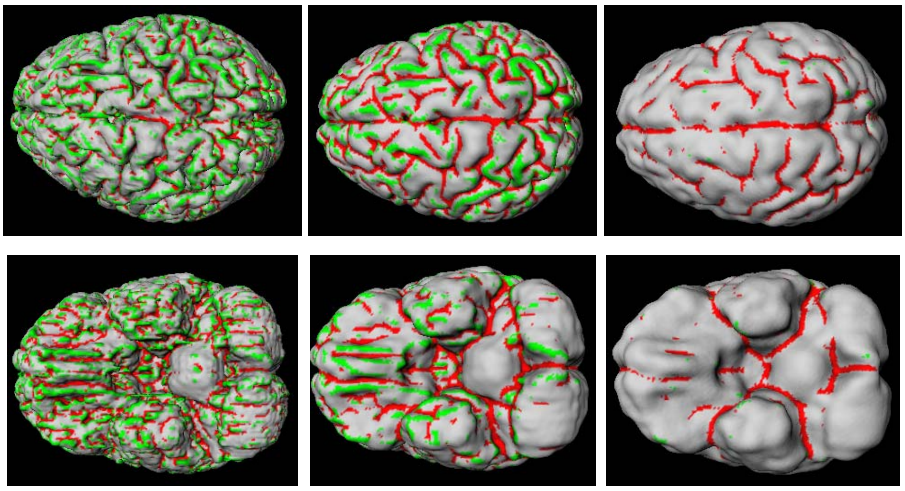

(a) scale 1 (b) scale 2 (c) scale 3

Figure 2: Sulci (red) and gyri (green) points of the study brain by thresholding the curvedness (Eq.(5)). Top: dorsal view; Bottom: ventral view. (a): scale 1 (Gauss smoothing $\sigma = 0.5$), sulci (35%), gyri (15%); (b): scale 2 (smoothing $\sigma = 1.5$), sulci (25%), gyri (10%); (c): scale 3 (smoothing $\sigma = 2.5$), sulci (10%), gyri (3%). (Note: the percentages shown in the brackets are the number of selected sulci or gyri points over the total number of surface points.)

The feature (curvedness) match measure used in Eq.(1) is formulated as:

$$f_{ij} = \begin{cases} 1.0, & \text{if } (t_i, t_j) = \begin{cases} \text{(sulcus, sulcus)} \\ \text{(gyrus, gyrus)} \\ \text{(no feature, no feature)} \end{cases} \\ 2.8, & \text{if } (t_i, t_j) = \begin{cases} \text{(sulcus, no feature)} \\ \text{(gyrus, no feature)} \end{cases} \\ 3.0, & \text{if } (t_i, t_j) = \text{(sulcus, gyrus)} \end{cases} \tag{8}$$

Thus, for each labeled point on the atlas, the point on the study surface which minimizes Eq.(1) within a radius $R_w$ (normally chosen to be 15 pixels) is selected as the corresponding

point.

### 3.2 Geodesic Path Computation

Given the set of corresponding points and their connections, the second step is to determine the shortest paths between each pair of connected surface points (Figure 3).

There are many methods to solve the shortest surface path finding problem [18, 19, 20, 32, 41]. The algorithm we use is based on Kimmel's two methods [18, 20], and is almost the same as his extended Fast Marching Method [20]. The Fast Marching Method [33, 34] is an extremely fast numerical algorithm for solving the Eikonal equation $\mid \nabla T \mid = \mathcal{F}(x, y)$ on a rectangular orthogonal mesh in $O(M \log M)$ steps, where $M$ is the total number of grid

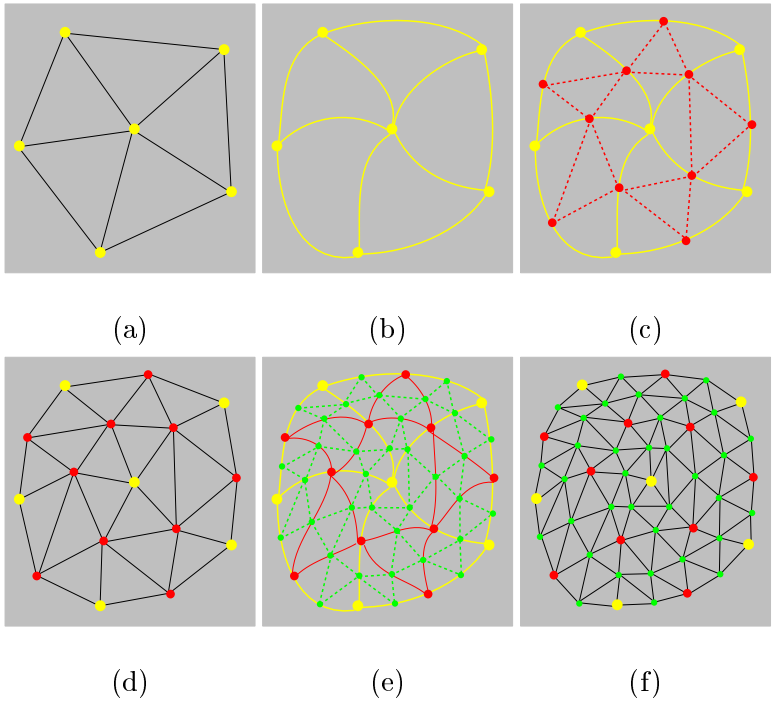


Figure 3: Diagram for corresponding surface points identification and surface triangulation in our hierarchical approach. (a): initial points and triangulation; (b): shortest paths between each pair of connected points; (c): selected mid-points on each shortest path (red dots) and triangle subdivision; (d): more dense triangulation; (e): repeating of (c) in a hierarchical way; (f): even more dense triangulation.

points. This technique has been extended to triangulated domains with the same computational complexity [20].

When we calculate the shortest path between two surface points, one is treated as the source point, and the other as the destination point. In our implementation, using this extended Fast Marching Method, we first solve the Eikonal equation with speed $\mathcal{F} = 1$ on the triangulated surface to compute the distance $T$ from a source point. Note that for all geodesic computations we use the original triangulated surface. Then, we backtrack along the gradient of the distance $T$ from the destination point. For each triangle, there is one gradient. We start from a point and "flow" inside the triangle which has the largest gradient according to the computed gradients. In this way, we get a sequence of straight segments, each segment corresponding to a path through one triangle. Since the original surface triangulation is done at the voxel level, the discrete path is fine enough to be a good approximation of the geodesic path on the continuous surface. In this way, the shortest path between the source and destination points is traced.

Figure 4 shows the Marching Cube triangulation [22] and two shortest paths for a synthetic surface.

(a) 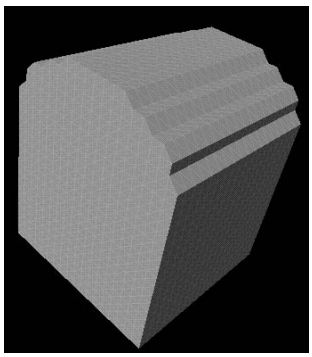 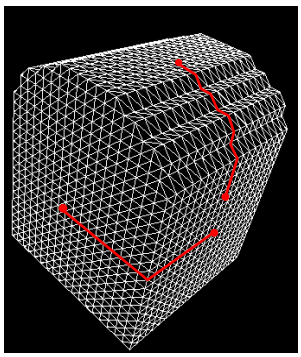 (b)

Figure 4: Shortest paths on a synthetic surface. (a): the synthetic surface (image size: $32 \times 32 \times 32$); (b): two shortest paths on the Marching Cube triangulated surface of (a).

### 3.3 Mid-point Selection and Triangle Subdivision

The third step of our approach is selecting the mid-point on each shortest path, and decomposing each triangle into four smaller ones (Figure 3(c)). In this way, a more dense triangulation is derived (Figure 3(a) and 3(d)).

### 3.4 Hierarchical Surface Reconstruction

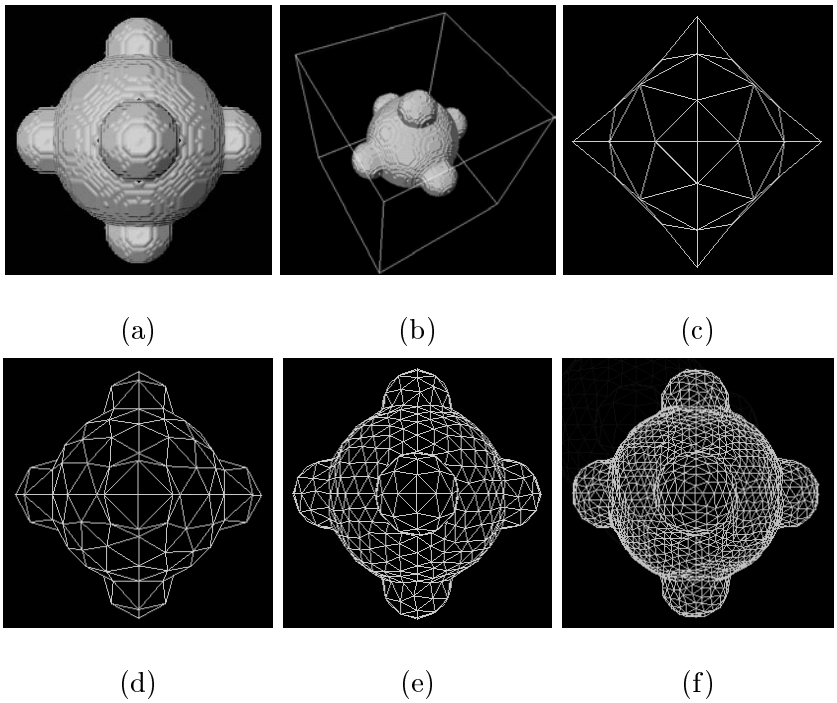

Figure 5: 3D synthetic surface reconstruction. (a): the synthetic surface (22, 782 points and 45, 560 triangles) (image size: $100 \times 100 \times 100$); (b): another view of (a); (c): initial points and triangulation (38 points and 72 triangles); (d) to (f): generated surface points and surface triangulation based on these points respectively after 1st, 2nd and 3rd iterations by our hierarchical approach (with number of points/triangles respectively: 146/288, 578/1152, 2306/4608).

Now, we simply repeat the previous two steps (Section 3.2 and Section 3.3) and thus generate even denser surface points and triangulation. Figure 3 diagrams our hierarchical strategy. We

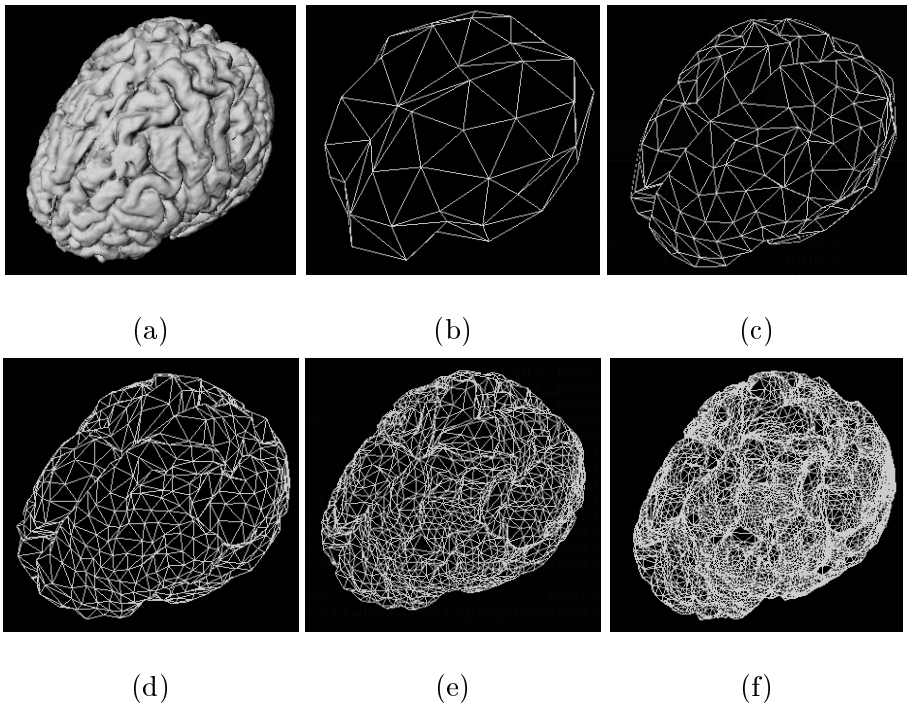


Figure 6: Brain surface reconstruction. (a): the original surface (164,477 points and 329,816 triangles); (b): initial points and triangulation (69 points and 134 triangles); (c) to (f): generated surface points and triangulation after 1st, 2nd, 3rd and 4th iterations by our hierarchical approach (with number of points/triangles respectively: 270/536, 1,074/2,144, 4,290/8,576, 17,154/34,304).

repeat this process until the triangles are small enough. Figure 5 shows a synthetic surface reconstruction example. Figure 6 shows a brain surface reconstruction process. As the iterations continue, more and more dense surface points and triangulation are derived. Note that since the number of identified corresponding points at each iteration is always the same for the atlas and study brains, the two surfaces are then matched at different scales.

## 4 Features of the Proposed Method

The assumption of our approach is that the relative deformation of the two surfaces is approximately a uniform stretching between the initial points. Locally uniform stretching, or homothetic

deformation [12] is a reasonable assumption and can be satisfied, at least approximately, by the appropriate selection of the initial points. The general requirement for the initial points labeling on the atlas surface is an even distribution. In areas of greater complexity, it may be necessary to include a denser distribution of initial points so that more accurate results can be derived. Deep sulcal areas have longer surface paths given the same Euclidean distance between the points.

Our initial points matching uses surface curvature, and the points interpolation is based on geodesics. Therefore, our approach can capture the global and local shape of the surface, which is the main advantage compared to other points matching algorithms [1, 27, 10]. Figure 7 shows schematically how the geodesic paths can follow brain sulci.

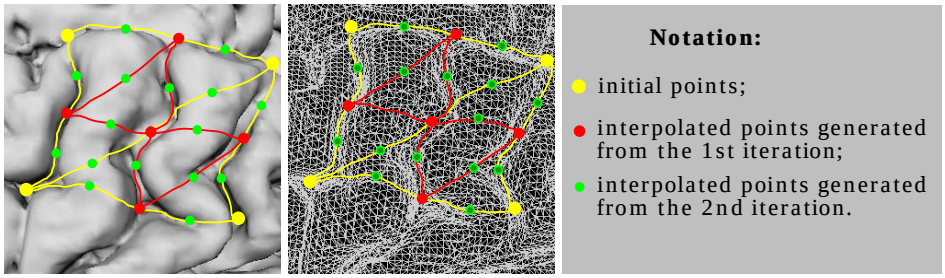


(a) (b) (c)

Figure 7: Schematic diagram showing brain sulci being followed. (a): geodesic paths and its mid-points on brain surface; (b): wire-frame version of (a); (c): notation for the diagram.

In our hierarchical closed surface reconstruction algorithm, if the number of initial points and triangles are respectively $P_0$ and $T_0$, then at $i$th iteration, the generated points, $P_i$, and triangles, $T_i$, are given by (see Appendix for detailed derivation):

$$P_i = P_0 + \frac{4^i - 1}{2} T_0; \qquad T_i = 4^i T_0 \tag{9}$$

Normally, surfaces are reconstructed to four iterations in our experiments.

# 5 Experiments and Evaluation

## 5.1 Real Pair of Atlas and Study Brains

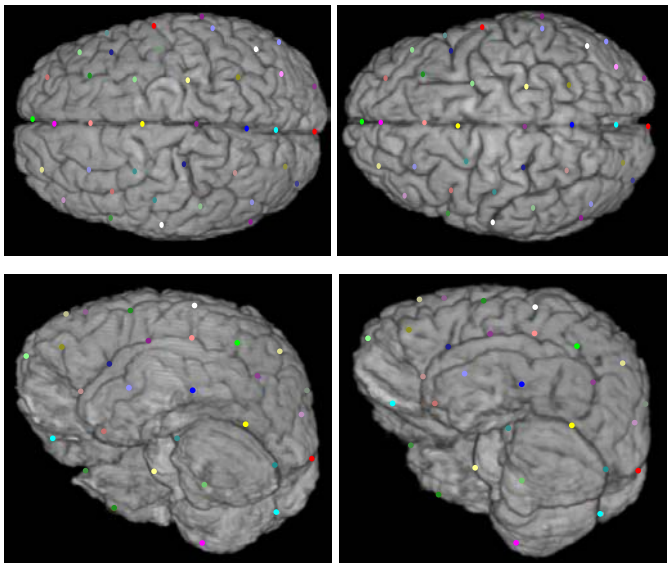

Figure 8: Automatically matched initial points on the brain surface (top and bottom are two different views). Left: atlas surface hand-labeled 69 points; Right: study surface corresponding 69 points identified by our automatic point matching procedure (Section 3.1).

Figure 8 shows the automatic points matching results on a pair of brain surfaces (Section 3.1). Regular sulcal and gyral points are identified consistently, as are the interhemispheric fissure points and points on the ventral surface at the brain stem and cerebellum. The consistent matching is due to the combined effect of the three measures (Eq.(2),(3),(8)) using the curvedness measure at three different scales.

Figures 9 and 10 demonstrate the surface correspondence and reconstruction process respectively for the atlas and study brains. The initial points for the atlas and study used in the iterations are shown in Figure 8. The dense mapping of the study and the atlas surfaces is then established by starting with the sparse initial corresponding points.

In order to evaluate our approach, we also implemented a simple closest point method for

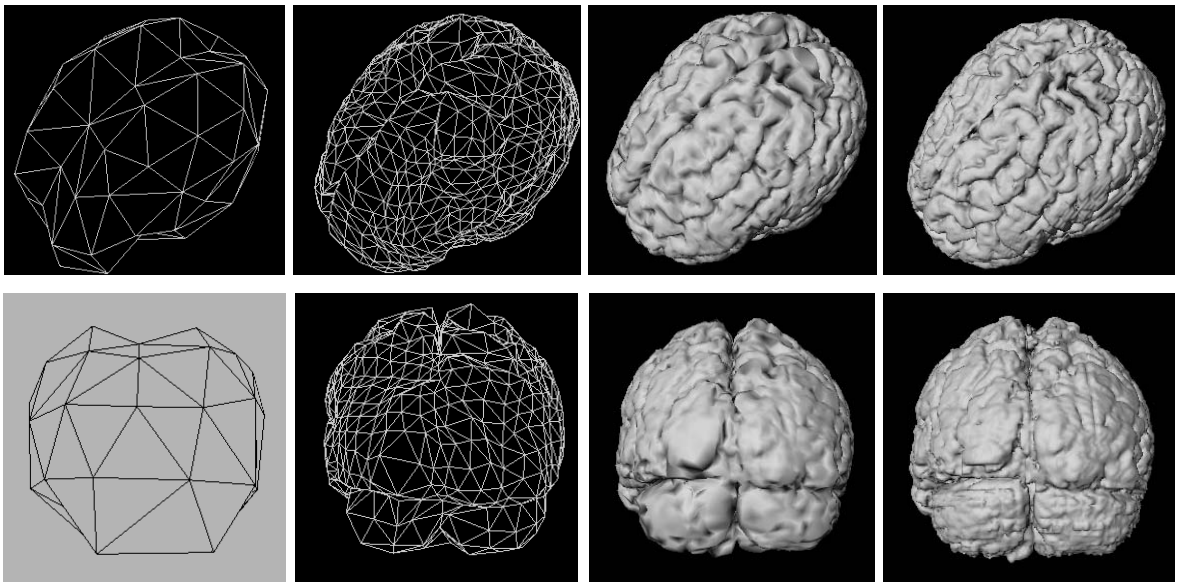

(a) (b) (c) (d)

Figure 9: Atlas surface correspondence and reconstruction by our shape-based approach (top and bottom are two different views). (a): initial points and triangulation (69 points and 134 triangles); (b): generated surface points and triangulation after 2nd iteration (1,074 points and 2,144 triangles); (c): reconstructed surface after the 4th iteration with normals extracted from the original surface (17,154 points and 34,304 triangles); (d): original atlas surface (187,969 points and 377,238 triangles).

surface matching. This method identifies the closest point on the study as the corresponding point for the atlas. By calculating the corresponding points of the reconstructed atlas after the 4th iteration (Figure 9(c)), we get the reconstructed study surface shown in Figure 12. Since the generated points for the atlas are roughly evenly distributed on the original atlas surface, the reconstructed surface in Figure 9(c) is a good approximation of the original one in Figure 9(d), with many visible sulci and gyri. We therefore expect that the corresponding points for the study should also reveal the sulcal and gyral pattern. From the top of Figures 10 and 12, it can be seen that our shape-based approach is able to generate more sulci and gyri on the reconstructed surface faithfully, resulting in a much better approximation of the original surface

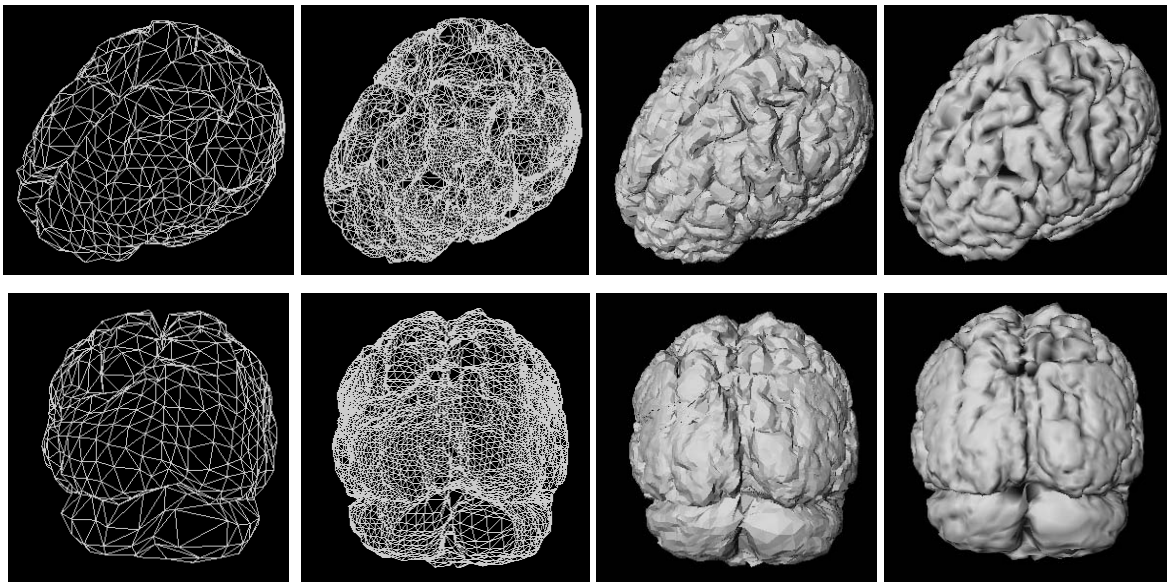

(a) (b) (c) (d)

Figure 10: Study surface correspondence and reconstruction by our shape-based approach (top and bottom are two different views). (a): generated surface points and triangulation after 2nd iteration (wire-frame); (b): generated surface points and triangulation after the 4th iteration; (c): reconstructed surface after the 4th iteration with normals computed from triangulation; (d): reconstructed surface after the 4th iteration with normals extracted from the original surface.

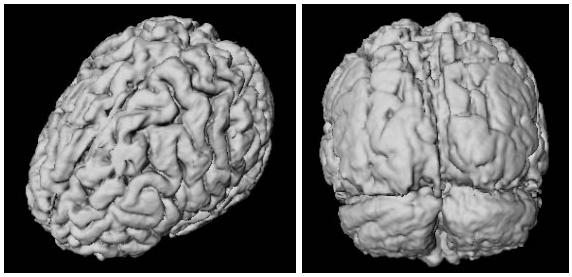

Figure 11: Two views of the original study surface (164, 477 points and 329, 816 triangles).

(Figure 11). The bottom of Figures 10 and 12 show that the simple closest point method can not give a reasonable posterior reconstructed surface. The difference in the posterior region can also be seen in Figure 13, where the five points in the atlas are corresponded well by our geodesic

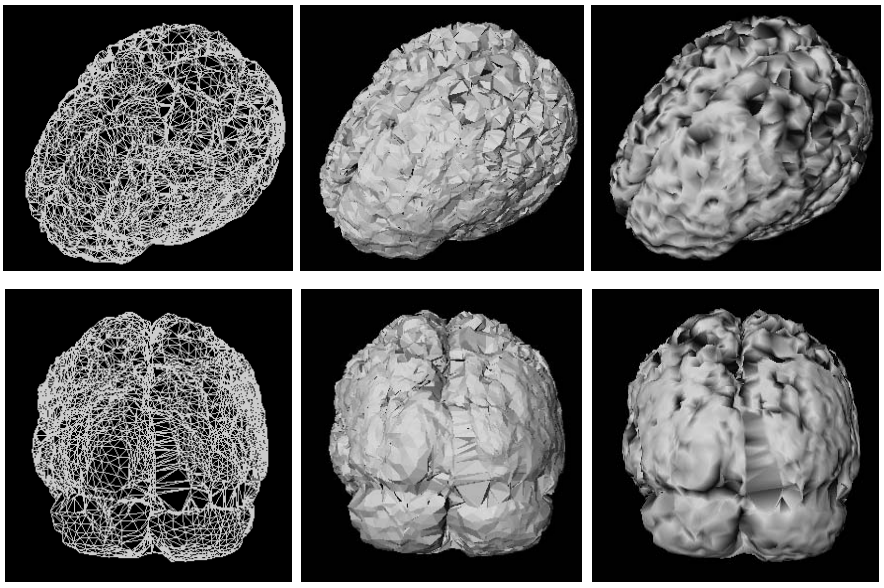

(a) (b) (c)

Figure 12: Study surface correspondence and reconstruction by simple closest point approach (top and bottom are two different views). (a): calculated corresponding surface points and projected triangulation of reconstructed atlas in Figure 9(c) (compare with Figure 10(b)); (b): reconstructed surface of (a) with normals computed from triangulation (compare with Figure 10(c)); (c): reconstructed surface of (a) with normals extracted from the original surface (compare with Figure 10(d)). Note, dark areas are due to the variation of the normals between the original surface (Figure 11) and the reconstructed surface in (b), and they show disagreement between the two surfaces.

method. The simple closest point method calculated the wrong corresponding points because the rigid and scaling transformation could not compensate for the deformation in the posterior part of the study brain.

### 5.2 Locally Deformed Atlas Brain

One major advantage of the proposed method is that it is able to capture the global and local shape of the surface, which can also be demonstrated in the experiment here. Shown in the top

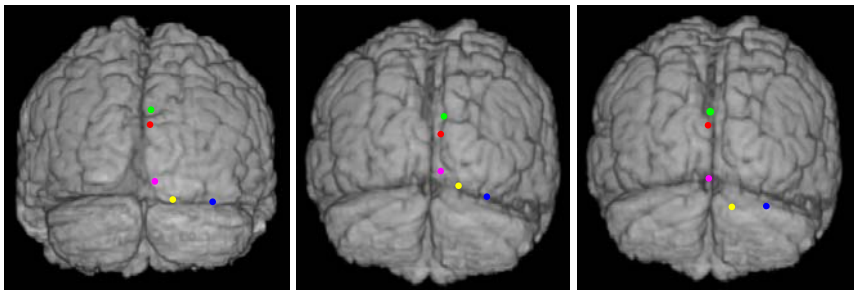

Figure 13: Located corresponding points comparison by different methods. Left: five points on the atlas posterior surface; Middle: the five corresponding points on the study surface by our shape-based method; Right: the five corresponding points on the study surface by the simple closest point method.

and bottom of Figure 14(a) are two deformed atlas brains with varying degrees of local bulging and denting. They are well reconstructed by using our shape-based surface matching (see Figure 14(b)). However, this can not be achieved by the simple closest point method, especially for large local deformation, as shown in Figure 14(c) and 14(d).

### 5.3 Real Atlas and Synthetically Warped Study

In order to further evaluate the method both quantitatively and qualitatively, we define a particular warp and apply it to the atlas brain image, generating a warped study image to which both our algorithm and the simple closest point algorithm can be applied. We use the following sinusoidal displacement fields for transforming the atlas image to a study image:

$$\begin{aligned} x_{new} &= x_{old} + A_x sin(\pi y_{old}/32); \\ y_{new} &= y_{old} + A_y sin(\pi z_{old}/32); \\ z_{new} &= z_{old} + A_z sin(\pi x_{old}/32) \end{aligned} \tag{10}$$

where $(x_{old}, y_{old}, z_{old})$ are coordinates of a point in the atlas image and $(x_{new}, y_{new}, z_{new})$ are coordinates of the corresponding point in the transformed study image. $A_x$, $A_y$, $A_z$ are the limits of the maximum displacement distances along the $x$, $y$, $z$ directions, respectively.

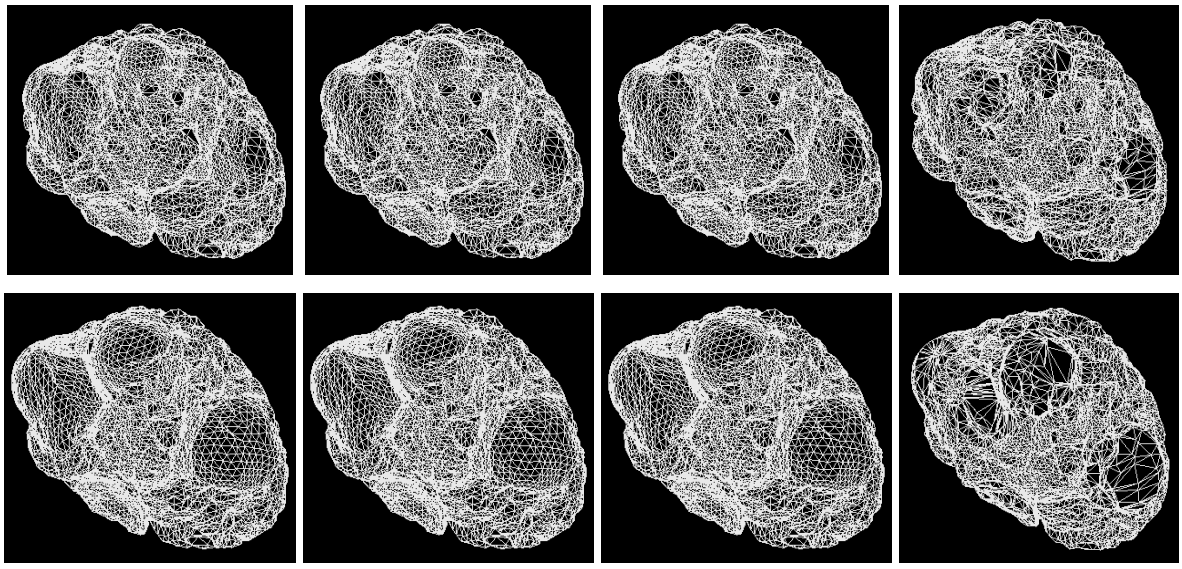

(a) (b) (c) (d)

Figure 14: Locally deformed atlas surface correspondence and reconstruction (top and bottom are different degrees of bulging and denting). (a): original locally deformed atlas surfaces; (b): reconstructed surfaces by our surface matching algorithm after 4th iteration; (c): wire-frames of (b) (our method); (d): wire-frames of reconstructed surfaces by simple closest point approach.

The transformed study image in this experiment is shown in Figure 15 bottom. The atlas initial points and triangulation are shown in Figure 9(a). The initial points of the study are derived either from the known warp, or from our automatic matching procedure described in Section 3.1. Using known initial points, the evaluation only reflects the comparison of our geodesic dense points correspondence algorithm and the simple closest point algorithm, and does not include the initial points matching step. Using the automatic matching procedure, the entire framework is evaluated.

By calculating the corresponding points of the reconstructed atlas after the 4th iteration (Figure 9(b)), we get the reconstructed study surfaces with different initial points and different methods shown in Figure 16. Clearly, our method gives better results no matter how the initial points are derived.

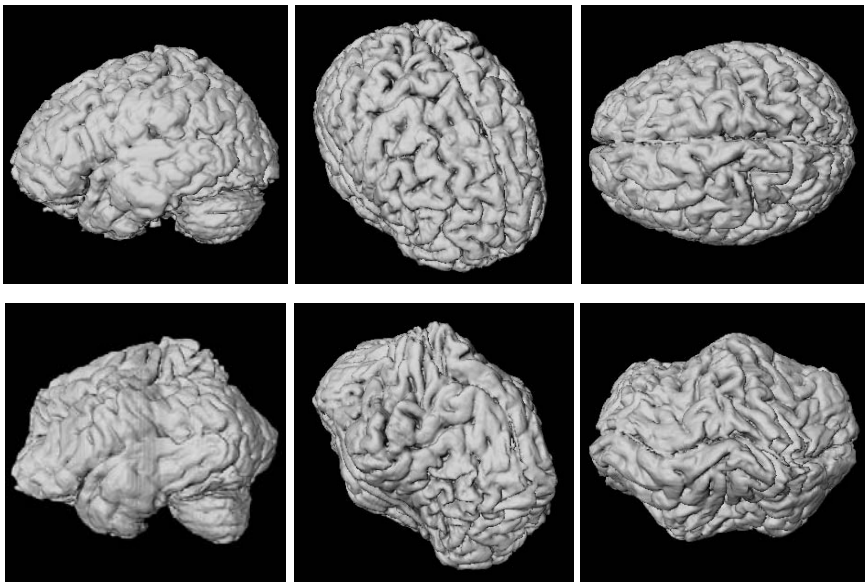

Figure 15: Atlas surface and synthetically warped study surface. Top: three views of the atlas surface (same brain as that in Figure 9(c)); Bottom: three views of the warped study surface by Eq.(10) with $A_x = A_y = A_z = 5.0$ ($154,080$ points and $308,808$ triangles).

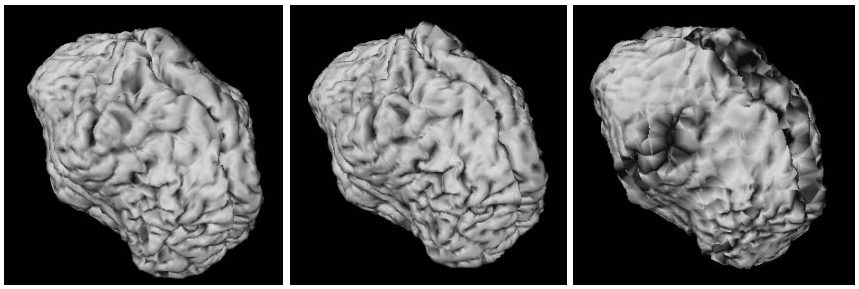

Figure 16: Reconstruction of the warped study surface (Figure 15 bottom) with different initial points and different methods. Left and Middle: by our shape-based method after the 4th iteration with initial points from known warp (left) and with initial points from our point matching procedure (middle); Right: by the simple closest point method.

Another way of examining the results, which is also useful for shape characterization, is to calculate the distance between each pair of points and visualize the distance as a color map on the study surface. Since the study here is warped from the true atlas by Eq.(10), we have the known distance map (Figure 17(a)) for evaluation. This color map is calculated and visualized

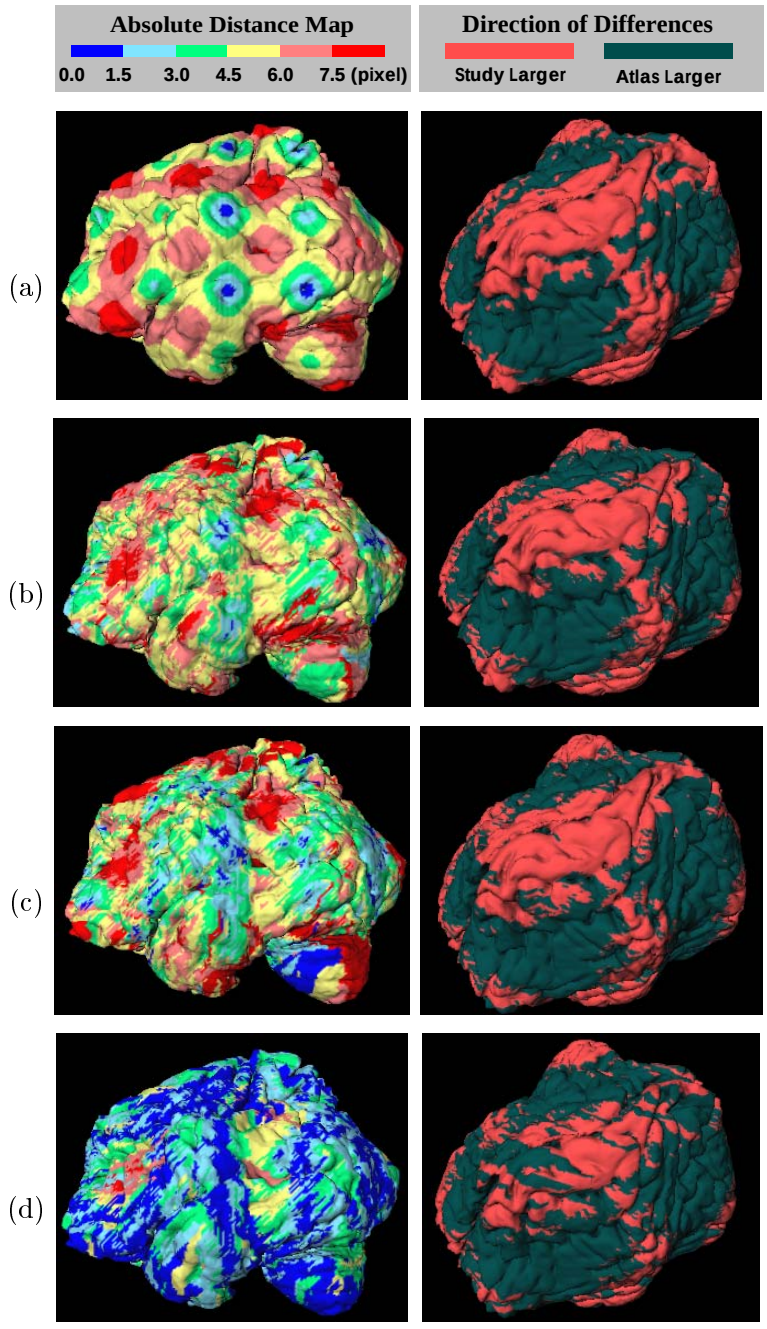


Figure 17: Evaluation of different methods for the known warp (Eq.(10)). (a): true absolute distance map and direction of differences (left and right are two different views); (b): results by our shape-based method (initial points from known warp) with absolute distance average error 1.9 pixels; (c): results by our shape-based method (initial points from our point matching procedure) with absolute distance average error 2.9 pixels; (d): results by the simple closest point method with absolute distance average error 4.0 pixels.

densely at each point on the study surface (154,080 points in total). For both methods, we first calculated the colored distance map at 17,154 points (the number of corresponding points for the atlas after the 4th iteration), and then used an iterative merging technique to color the remaining study surface points. The average error of the absolute distance to the true distance map is evaluated at the calculated 17,154 points. From the results in Figure 17, we can see that the displacement pattern and mean square distance error for our method (Figure 17(b),(c)) are much better than for the simple closest point method (Figure 17(d)). The simple closest point approach tends to give smaller absolute distances than the true distance, while our shape-based approach results in more accurate distances comparable to the true distance.

## 6 Conclusions and Future Directions

We have presented a new shape-based approach for 3D brain surface matching using geodesic paths and geometrical features. The entire process of our method is automatic except for the atlas initial critical points labeling and initial triangulation construction, which need to be done only once for the atlas. By minimizing the objective function which incorporates local surface geometry, the initial points on the study surface are identified and matched. The corresponding surface points are generated by labeling mid-points on the shortest paths recursively. Surface correspondence and triangulation are computed simultaneously by using a hierarchical scheme. Experimental results and evaluation further demonstrate that our method performs well for surface matching and surface shape recovery.

The directions of future research include: incorporating other attributes and coarse to fine search for initial points matching; further validation on large amount of brain images; and using generated corresponding surface points as landmarks for 3D statistical model building and surface based volumetric non-rigid registration.

### Appendix — Number of Generated Points and Triangles

In our hierarchical closed surface reconstruction algorithm, the complexity of the final triangulation is related to the initial triangulation and the number of iterations. For a closed surface, the number of triangle edges, $E$, is related to the number of triangles by $E = 3T/2$. If $P_i$, $T_i$ and $E_i$ are respectively the number of points, triangles, and edges at the $i$th iteration ($i = 1, 2, 3, \ldots$), we have:

$$\begin{aligned} E_i &= \frac{3}{2} T_i \\ T_i &= 4T_{i-1} = 4^i T_0 \\ E_i &= 6T_{i-1} = 6 \cdot 4^{i-1} T_0 \end{aligned} \tag{11}$$

because each triangle is divided into four at each iteration. Also note that $E_i = 4^i E_0$.

Since the points are generated by labeling one mid-point on each surface path ended with two vertices of a triangle, then:

$$P_i = P_{i-1} + E_{i-1} = (P_{i-2} + E_{i-2}) + E_{i-1} = P_0 + \sum_{n=0}^{i-1} E_n \tag{12}$$

Substituting Eq.(11) into Eq.(12), we have:

$$P_i = P_0 + \sum_{n=0}^{i-1} 6 \cdot 4^{n-1} T_0 = P_0 + \frac{4^i - 1}{2} T_0 \tag{13}$$

## References


[1] P. J. Besl and N. D. McKay, A method for registration of 3-D shapes, *IEEE Transactions on Pattern Analysis and Machine Intelligence* **14**(2), 1992, 239-256.

[2] F. L. Bookstein, Landmark methods for forms without landmarks: Morphometrics of group differences in outline shape, *Medical Image Analysis* **1**(3), 1997, 225-243.

[3] A. D. Brett, A. Hill and C. J. Taylor, A method of 3D surface correspondence and interpolation for merging shape examples, *Image and Vision Computing* **17**(8), 1999, 635-642.

[4] M. P. do Carmo, *Differential Geometry of Curves and Surfaces*, Prentice-Hall, New Jersey, 1976.

[5] A. Caunce and C. J. Taylor, Using local geometry to build 3D sulcal models, in *Information Processing in Medical Imaging*, LNCS 1613, Springer, Berlin, 1999, pp. 196-209.

[6] G. E. christensen, R. D. Rabbitt and M. I. Miller, Deformable templates using large deformation kinematics, *IEEE Transactions on Image Processing* **5**(10), 1996, 1435-1447.

[7] C. Davatzikos, Spatial transformation and registration of brain images using elastically deformable models, *Computer Vision and Image Understanding* **66**(2), 1997, 207-222.

[8] J. S. Duncan, R. L. Owen, L. H. Staib and P. Anandan, Measurement of non-rigid motion in images using contour Shape descriptors, in *Proceedings of the IEEE Conference on Computer Vision and Pattern Recognition*, 1991, pp. 318-324.

[9] J. Feldmar, G. Malandain, J. Declerck and N. Ayache, Extension of the ICP algorithm to non-rigid intensity-based registration of 3D volumes, in *Proceedings of the IEEE Workshop on Mathematical Methods in Biomedical Image Analysis*, June 1996, pp. 84-93.

[10] M. Fleute and S. Lavallée, Building a complete surface model from sparse data using statistical shape models: Application to computer assisted knee surgery, in *First International Conference on Medical Image Computing and Computer-Assisted Intervention*, LNCS 1496, Springer, Berlin, October 1998, pp. 879-887.

[11] J. C. Gee, C. Barillot, L. L. Briquer, D. R. Haynor and R. Bajcsy, Matching structural images of the human brain using statistical and geometrical image features, in *Proceedings of SPIE Visualization in Biomedical Computing 1994*, Vol. 2359, 1994, pp. 191-204.

[12] D. B. Goldgof, H. Lee and T. S. Huang, Motion analysis of nonrigid surfaces, in *Proceedings of the IEEE Conference on Computer Vision and Pattern Recognition*, June 1988, pp. 375-380.

[13] L. D. Griffin, The intrinsic geometry of the cerebral cortex, *Journal of Theoretical Biology* **166**(3), 1994, 261-273.

[14] R. C. Gur, P. D. Mozley, S. M. Resnick, et al., Gender differences in age effect on brain atrophy measured by magnetic resonance imaging, in *Proceedings of National Academy of Sciences*, Vol. 88, April 1992, pp. 2845–2849.

[15] R. C. Gur, B. I. Turetsky, M. Matsui, M. Yan, W. Bilker, P. Hughett, and R. E. Gur, Sex differences in brain gray and white matter in healthy young adults: Correlations with cognitive performance, *Journal of Neuroscience* **19**(10), May 1999, 4065–4072.

[16] H. J. Jiang, R. A. Robb and K. S. Holton, A new approach to 3-D registration of multimodality medical images by surface matching, in *Visualization in Biomedical Computing 1992, Proceedings of SPIE 1808*, 1992, pp. 196-213.

[17] N. Khaneja, M. I. Miller and U. Grenander, Dynamic programming generation of curves on brain surfaces, *IEEE Transactions on Pattern Analysis and Machine Intelligence* **20**(11), 1998, 1260-1265.

[18] R. Kimmel, A. Amir and A. M. Bruckstein, Finding shortest paths on surfaces using level sets propagation, *IEEE Transactions on Pattern Analysis and Machine Intelligence* **17**(6), 1995, 635-640.

[19] R Kimmel and N Kiryati, Finding shortest paths on surfaces by fast global approximation and precise local refinement, *International Journal of Pattern Recognition and Artificial Intelligence* **10**(6), 1996, 643-656.

[20] R. Kimmel and J. A. Sethian, Computing Geodesic Paths on Manifolds, *Proceedings of National Academy of Sciences* **95**(15), 1998, 8431-8435.

[21] J. J. Koenderink and A. J. van Doorn, Surface shape and curvature scales, *Image and Vision Computing* **10**(8), 1992, 557-565.

[22] W. E. Lorensen and H. E. Cline, Marching cubes: A high resolution 3D surface construction algorithm, *Computer Graphics* **21**(4), 1987, 163-169.

[23] J. McEachen and J. S. Duncan, Shape-based tracking of left ventricular wall motion, *IEEE Transactions on Medical Imaging* **16**(3), June 1997, 270-283.

[24] M. Narayan, E. Anderson, A. Goddard, S. Woods, L. H. Staib, D. S. Charney, and J. D. Bremner, Temporal lobe volume in panic disorder: A quantitative magnetic resonance imaging study, *Psychiatry Research: Neuroimaging*, 2000 (in press).

[25] P. Nopoulos, M. Flaum, D. O'Leary, and N. C. Andreasen, Sexual dimorphism in the human brain: evaluation of tissue volume, tissue composition and surface anatomy using magnetic resonance imaging, *Psychiatry Research: Neuroimaging* **98**(1), 2000, 1-13.

[26] B. S. Peterson, B. Vohr, L. H. Staib, C. Cannistraci, A. Dolberg, K. A. Schneider, K. H. Katz, M. Westerveld, S. Sparrow, A. Anderson, C. Duncan, R. W. Makuch, J. C. Gore, and L. R. Ment, Regional brain volume abnormalities are associated with long-term cognitive outcome in preterm infants, *J. Am. Med. Assoc.*, 2000 (in press).

[27] A. Rangarajan, H. Chui and F. L. Bookstein, The softassign Procrustes matching algorithm, in *Information Processing in Medical Imaging*, LNCS 1230, Springer, Berlin, June 1997, pp. 29-42.

[28] L. Regeur, Increasing loss of brain tissue with increasing dementia: A stereological study of post-mortem brains from elderly females, *European Journal of Neurology* **7**(1), January 2000, 47-54.

[29] M. E. Rettmann, X. Han and J. L. Prince, Watersheds on the cortical surface for automated sulcal segmentation, in *Proceedings of the IEEE Workshop on Mathematical Methods in Biomedical Image Analysis*, June 2000, pp. 20-27.

[30] B. M. ter Haar Romeny, L. M. J. Florack, A. H. Salden and M. A. Viergever, Higher order differential structure of images, *Image and Vision Computing* **12**(6), 1994, 317-325.

[31] R. T. Schultz, N. K. Cho, L. H. Staib, L. E. Kier, J. M. Fletcher, S. E. Shaywitz, D. P. Shankweiler, J. C. Gore, J. S. Duncan, and B. A. Shaywitz, Brain morphology in normal and dyslexic children: The influence of sex and age, *Ann. Neurol.* **35**(6), June 1994, 732-742.

[32] E. L. Schwartz, A. Shaw and E. Wolfson, A numerical solution to the generalized mapmaker's problem: flattening nonconvex polyhedral surfaces, *IEEE Transactions on Pattern Analysis and Machine Intelligence* **11**(9), 1989, 1005-1008.

[33] J. A. Sethian, A fast marching level set method for monotonically advancing fronts, *Proceedings of the National Academy of Sciences* **93**(4), 1996, 1591-1595.

[34] J. A. Sethian, *Level Set Methods: Evolving Interfaces in Geometry, Fluid Mechanics, Computer Vision and Materials Science*, Cambridge University Press, 1996.

[35] D. Shen and C. Davatzikos, HAMMER: Hierarchical attribute matching mechanism for elastic registration, in *Proceedings of the IEEE Workshop on Mathematical Methods in Biomedical Image Analysis*, December 2001, pp. 29-36.

[36] P. Shi, G. Robinson, A. Chakraborty, L. H. Staib, R. Constable, A. Sinusas and J. S. Duncan, A unified framework to assess myocardial function from 4D images, *Computer Vision, Virtual Reality and Robotics in Medicine*, LNCS 905, Springer, Berlin, 1995, 327-340.

[37] W. G. Staal, H. E. Hulshoff Pol, H. G. Schnack, M. L. Hoogendoorn, K. Jellema, and R. S. Kahn, Structural brain abnormalities in patients with schizophrenia and their healthy siblings, *American Journal of Psychiatry* **157**(3), March 2000, 416-421.

[38] H. Tagare, Shape-based nonrigid correspondence with applications to heart motion analysis, *IEEE Transactions on Medical Imaging* **18**(7), 1999, 570-579.

[39] P. Thompson and A. W. Toga, A surface-based technique for warping three-dimensional image of the brain, *IEEE Transactions on Medical Imaging* **15**(4), August 1996, 402-417.

[40] M. Vaillant and C. Davatzikos, Hierarchical matching of cortical features for deformable brain image registration, in M. Šámal A. Kuba and A. Todd-Pokropek, editors, *Information Processing in Medical Imaging*, LNCS 1613, Springer, Berlin, 1999, pp. 182-195.

[41] E. Wolfson and E. L. Schwartz, Computing minimal distances on polyhedral surfaces, *IEEE Transactions on Pattern Analysis and Machine Intelligence* **11**(9), 1989, 1001-1005.

[42] Y. Wang, B. S. Peterson and L. H. Staib, Shape-based 3D surface correspondence using geodesics and local geometry, in *Proc. IEEE Conf. on Computer Vision and Pattern Recognition*, Vol. II, June 2000, pp. 644-651.

[43] X. Zeng, L. H. Staib, R. T. Schultz and J. S. Duncan, Segmentation and measurement of the cortical from 3D MR images, in *First International Conference on Medical Image Computing and Computer-Assisted Intervention*, LNCS 1496, Springer, Berlin, October 1998, pp. 519-530.

[44] X. Zeng, L. H. Staib, R. T. Schultz, H. Tagare and J. S. Duncan, A new approach to 3D sulcal ribbon finding from MR images, in *Second International Conference on Medical Image Computing and Computer-Assisted Intervention*, LNCS 1679, Springer, Berlin, October 1999, pp. 148-157.